

## Optimization of finned solar photovoltaic phase change material (finned pv pcm) system



Sourav Khanna<sup>a,\*</sup>, K.S. Reddy<sup>b</sup>, Tapas K. Mallick<sup>a,\*\*</sup>

<sup>a</sup> Environment and Sustainability Institute, Penryn Campus, University of Exeter, Cornwall TR10 9FE, United Kingdom

<sup>b</sup> Heat Transfer and Thermal Power Laboratory, Department of Mechanical Engineering, Indian Institute of Technology Madras, Chennai 600 036, India

### ARTICLE INFO

#### Keywords:

Phase change material  
Photovoltaic  
Thermal management  
Optimization  
Fin

### ABSTRACT

Heat generation during the operation of the photovoltaic (PV) cell raises its temperature and results in reduced electrical output. The heat produced in the process can be removed by attaching phase change material (PCM) at the back of the PV panel which can contain the PV temperature substantially and increase its efficiency. Fins can be used inside the PCM container to enhance the heat transfer. In literature, it is observed that as soon as PCM is melted completely, the heat extraction rate of PCM reduces which again leads to increase in PV temperature. However, the study carrying out the optimization of Finned-PV-PCM system to keep PV temperature low during operation for different solar irradiance levels is not available in literature. Thus, in the current study, the most suitable depth of PCM container is calculated for different solar irradiance levels. In addition, how it is affected with spacing between successive fins, fin length and fin thickness has been studied. The best fin dimensions are also calculated. The results show that the most suitable depth of PCM container is 2.8 cm for  $\Sigma I_T = 3 \text{ kWh/m}^2/\text{day}$  and 4.6 cm for  $\Sigma I_T = 5 \text{ kWh/m}^2/\text{day}$  for the chosen parameters. The best spacing between successive fins (to keep PV temperature low) is 25 cm, best fin thickness is 2 mm and best fin length is the one when it touches the bottom of the container. PV, PV-PCM and Finned-PV-PCM systems are also compared. For PV-PCM system (without fins), the most suitable depth of PCM container is 2.3 cm for  $\Sigma I_T = 3 \text{ kWh/m}^2/\text{day}$  and 3.9 cm for  $\Sigma I_T = 5 \text{ kWh/m}^2/\text{day}$ .

### 1. Introduction

PV cells can convert only a fraction of the incident solar radiation into electricity. A major fraction is converted into heat and raises the temperature of the cell. The temperature rise reduces the solar to electricity conversion efficiency of the cell [1]. The studies involving phase change material (PCM) for extracting heat from PV have been reviewed.

Some works on experimental investigation of the photovoltaic-phase change material system are summarized. Huang et al. [2] have compared the performance of photovoltaic-phase change material system with fins and no fins inside the PCM container using RT25 and GR40 PCMs. The results show that the deployment of fins can reduce the PV temperature. Hasan et al. [3] have compared the behaviour of the system using five different PCMs: paraffin wax (RT20), capric-lauric acid (C-L), capric-palmitic acid (C-P), pure salt hydrate ( $\text{CaCl}_2 \cdot 6\text{H}_2\text{O}$ ) and commercial blend (SP22). It has been shown that the photovoltaic temperature can be decreased by 18 °C maximally at 1000 W/m<sup>2</sup> using C-P and  $\text{CaCl}_2 \cdot 6\text{H}_2\text{O}$ . Indartono et al. [4] have

proposed a yellow petroleum jelly as PCM for the operation and studied the performance of the system under the climate of Indonesia. An increment in photovoltaic efficiency from 8.3% to 10.1% has been observed. Mahamudul et al. [5] have considered RT35 PCM and carried out the study for the climate of Malaysia. The results show a decrement of 10 °C in the photovoltaic temperature using PCM. Park et al. [6] have varied the thickness of PCM layer and analysed the performance of the system for the weather of South Korea. A maximum increment of 3% in the electrical efficiency is achieved. Hasan et al. [7] have compared the behaviour of the system at two different locations: Ireland and Pakistan. The performance of the system is better at Pakistan. Hasan et al. [8] investigated the system's behaviour under extremely hot weather of the United Arab Emirates. An increase of 5.9% in the annual electricity generation is achieved. Sharma et al. [9] have integrated the RT42 phase change material in building integrated concentrated photovoltaic and reported an increase of 7.7% in the electrical efficiency at 1000 W/m<sup>2</sup>. Huang et al. [10] have worked on investigating the system's performance considering crystalline segregation of PCM. Waksol A, RT27 and RT35 phase change materials have been considered for the

\* Corresponding author.

\*\* Corresponding author.

E-mail addresses: [s.khanna@exeter.ac.uk](mailto:s.khanna@exeter.ac.uk) (S. Khanna), [t.k.mallick@exeter.ac.uk](mailto:t.k.mallick@exeter.ac.uk) (T.K. Mallick).

**Nomenclature**

$B$	liquid fraction of the phase change material during phase transition
$C$	constant appeared in Eq. (31)
$c_p$	specific heat capacity (J/kgK)
$D$	function used to distribute the latent heat in phase change zone
$F$	view factor
$g$	gravitational acceleration ( $m/s^2$ )
$G$	portion of solar irradiance converted into heat ( $W/m^3$ )
$Gr_c$	critical Grashof number
$h$	heat transfer coefficient due to convection ( $W/m^2K$ )
$I_T$	instantaneous solar-irradiance on tilted plane ( $W/m^2$ )
$k$	thermal conductivity ( $W/mK$ )
$L_{ch}$	characteristic length (m)
$L_f$	length of fins (m)
$L_h$	latent heat (J/kg)
$Nu$	Nusselt number
$p$	pressure of phase change material (Pa)
$Pr$	Prandtl number of air
$q$	constant appeared in Eq. (31)
$q_L$	rate of heat loss ( $W/m^2$ )
$Ra$	Rayleigh number
$Re_c$	critical Reynolds number
$s_f$	spacing between successive fins (m)
$S_h$	solar irradiance transformed into heat ( $W/m^2$ )
$t$	time (s)
$t_f$	thickness of fins (m)
$T$	temperature (K)
$T_m$	melting point of phase change material (K)
$u$	phase change material's velocity (m/s)
$v_w$	velocity of wind (m/s)
$x_c$	critical length (m)

**Greek symbols**

$\beta$	inclination angle of the system (rad)
---------	---------------------------------------

$\beta_c$	coefficient for expansion of phase change material due to temperature ( $/K$ )
$\gamma_w$	wind azimuth angle (rad)
$\delta$	depth of the box containing phase change material (m)
$\Delta T$	region of phase change (K)
$\varepsilon$	emissivity for reradiation
$\eta_{PV}$	electrical efficiency of the photovoltaic
$\mu$	phase change material's dynamic viscosity (kg/ms)
$\rho$	density of the material ( $kg/m^3$ )
$\sigma$	Stefan–Boltzmann constant ( $W/m^2 K^4$ )
$(\tau\alpha)_{eff}$	effective product of transmissivity of glass cover and absorptivity of solar cell
$\nu$	kinematic viscosity of air ( $m^2/s$ )

**Abbreviation**

EVA	ethylene vinyl acetate
PCM	phase change material
PV	panel of photovoltaic cells

**Subscripts**

a	ambient
al	aluminium
avg	averaged
b	bottom surface of PV
f	forced
g	ground
gl	glass layer
l	liquidus
n	natural
P	phase change material's layer
s	solidus; sky
t	photovoltaic top surface
ted	tedler layer
x	x direction
y	y direction
z	z direction

investigation. It is reported that the fins inside the PCM container can improve the performance. Browne et al. [11,12] have developed a pipe network inside the phase change material's container so that the storage of heat can be utilized using the flow of water through the pipes and achieved a thermal efficiency of 20%. Hachem et al. [13] have investigated the performance of photovoltaic integrated with mixed phase change material (copper, petroleum jelly and graphite powder) and pure phase change material and average increase of 5.8% and 3% respectively in the electrical efficiency have been reported. Several review works [14–18] also discuss the behaviour of photovoltaic-phase change material system.

Not just experimental work but several numerical studies have also been conducted for the thermal analysis of the PV-PCM system. Brano et al. [19] have used a finite difference method to analyse the thermal performance of the system considering RT27 PCM and found that the calculated values of the PV temperature differ from the measured ones by 7%. Atkin and Farid [20] have integrated the PCM with heat sink for PV cooling and shown a 12.97% enhancement in the photovoltaic electrical efficiency. Smith et al. [21] have estimated the power generation by photovoltaic-phase change material system across countries and found that the PCM integration for cooling of the PV is best for tropical regions. Kibria et al. [22] have used three phase change materials viz. RT20, RT25 and RT28HC and analysed the behaviour of the system and achieved an increase of 5% in the electrical efficiency.

All previous numerical studies ignored convection inside the melted

PCM which certainly has a considerable impact on the performance of photovoltaic-phase change material system [23]. The following works include convection. Huang et al. [24] have analysed the photovoltaic-phase change material system for two cases, fins and without fins, inside the container considering RT25 PCM. The results show that the introduction of fins can reduce the PV temperature by 3 °C. Ho et al. [25] investigated the photovoltaic coupled with microencapsulated phase change material and found an increment in the photovoltaic electrical efficiency from 19.1% to 19.5%. Huang [26] has investigated the thermal behaviour of the system using combination of PCMs considering RT21, RT27, RT31 and RT60. RT27-RT21 combination yields better performance. Khanna et al. [27–29] have studied the effect of operating conditions on the performance of photovoltaic-phase change material system and found that the increase in the tilt of system leads to increase in the melting rate of PCM. To encounter the sudden changes in the thermal properties of PCM during phase change in the convergence of the numerical solution, Biwole et al. [30] and Groulx and Biwole [31] have implemented Dirac delta function for modelling the rapid change in the specific heat of PCM.

The aim of the above studies is to enhance the PV efficiency. Many studies are available aiming at the improvement of heat transfer inside the PCM using fins: Shatikian et al. [32] have reported that the lesser spacing/thickness of fins leads to quicker melting of PCM (keeping spacing to thickness ratio fixed) which is due to the increase in the number/surface area of fins. The simulations have been carried out for

constant wall temperature where as Shatikian et al. [33] have carried out the simulations for constant heat flux. Saha and Dutta [34] have optimized the thickness and number of fins to maximize the operational time of heat sink for the prescribed heat flux and the critical chip temperature. Nayak et al. [35] have investigated the performance of phase change material using porous matrix, plate-type fins and rod-type fins. It is found that the rod-type fins perform better than plate-type ones. Baby and Balaji [36] have analysed the PCM and fins based heat sink for the thermal management of the portable electronic devices. The operational time is enhanced by a factor of 18 for the pin fin heat sink as compared to the heat sink without fin. Fok et al. [37] have also carried out the thermal management of the portable electronic devices using PCM in the finned heat sink. It has been found that the increase in the number of fins leads to better heat dissipation. Fan et al. [38] have analysed the effect of PCM melting temperature on the performance of Finned-PCM heat sink for the thermal management of electronics. It is found that the PCM with higher melting temperature can increase the protection time of the devices from over-heating. However, it is also reported that the PCM with lower melting temperature enables a prompt protection of the devices. Srikanth and Balaji [39] have investigated the behaviour of the Finned-PCM heat sink subjected to non-uniform heat loading using four discrete heaters. It is found that the non-uniform heat flux highly affects the melting and solidification cycle. A multi objective optimization have been carried out to maximize the charging period and minimize the discharging period of the heat sink simultaneously. Biwole et al. [40] have recently carried out a detailed study to analyse the impact of fin size on the PCM performance. It is concluded that the system performs better when fins touch the back of the PCM container and the increase in the number of fins reduces the standard deviation of the front plate temperature.

From the available studies, it is observed that once the phase change material melts completely, the rate of heat extraction by phase change material decreases which again leads to rapid increase in PV temperature. Thus, the current work aims at computing the most suitable depth of phase change material's container to keep photovoltaic cool in desired temperature range for different daily solar radiation, spacing between successive fins, length and thickness of fins. The best fin dimensions are also calculated to maintain the photovoltaic at low temperature.

## 2. Methodology

Three types of systems have been chosen for the present work as shown in Fig. 1. First system consists of a photovoltaic panel. Second system consists of a photovoltaic panel equipped with a phase change material's container (aluminium box) at the back. In the third system, aluminium fins are introduced inside the PCM container. The tilt angles of the systems are denoted by  $\beta$ . The PV panel is a stack of five layers. The depth and length of the phase change material's container are represented by  $\delta$  and  $L$ . Aluminium fins have been deployed equidistantly at the top wall of the container with spacing between successive fins as  $s_f$ .  $L_f$  and  $t_f$  respectively represent the length and the thickness of the fins. The side walls and the bottom of the PCM chamber are assumed to be thermally insulated.

The following assumptions have been made for the work.

- (i) The solar irradiance incident on the photovoltaic is distributed uniformly across the surface as the top surface is considered as perfectly clean to avoid the effect of dirt and clear sky conditions are considered to avoid the non-uniformity caused due to clouds
- (ii) Since the individual layers of PV are very thin, they are considered to be homogenous and isotropic
- (iii) The presence of fins can reduce the adverse effect of crystalline segregation of phase change material. Thus, the PCM in solid and liquid phases is assumed as homogeneous and isotropic
- (iv) Since the operating temperature range is not too wide, the thermal

- properties of the PV and phase change material (in same phase) are considered to be unaffected with change in temperature
- (v) Since the bottom and the side walls of the system are thermally insulated, the heat losses from them are neglected
- (vi) Due to the symmetry of the system along the  $z$  direction and the side walls of the system are thermally insulated, two-dimensional study has been carried out

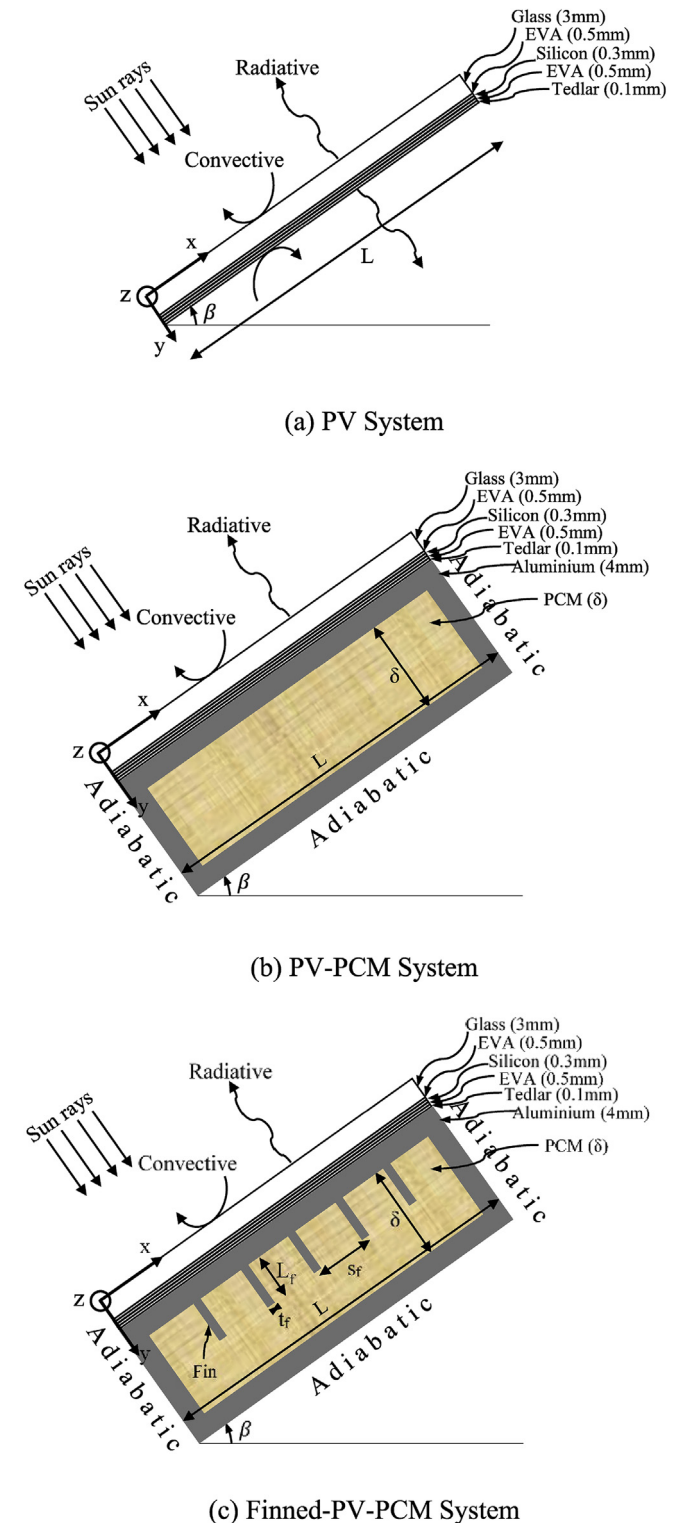


Fig. 1. Systems considered for the present study.

A major fraction of the solar radiation reaching the PV panel ( $I_T$ ) is transmitted through the glass cover. The fraction that is absorbed by the solar cell can be written in terms of effective product of transmissivity of glass cover and absorptivity of the solar cell as  $(\tau\alpha)_{eff} \times I_T$ .  $(\tau\alpha)_{eff} = 0.9$  [41] is taken for the current work. A fraction of the absorbed energy is converted into electrical energy and the rest is transformed into heat ( $S_h$ ) which is given by

$$S_h = (\tau\alpha)_{eff} I_T - \eta_{PV} I_T \tag{1}$$

where  $\eta_{PV}$  is the electrical efficiency of the PV which is represented as a function of PV averaged temperature ( $T_{PV,avg}$ ) and  $I_T$ . For the current work, it is taken as  $\eta_{PV} = 0.20 [1 - 0.005 (T_{PV,avg} - 25)] + 0.085 \ln (I_T / 1000)$  [41]. The negative coefficient of  $T_{PV,avg}$  in this correlation conveys that the PV efficiency decreases with increase in its temperature and the positive coefficient of  $I_T$  conveys that the efficiency increases with increase in the incident solar radiation. Of the total heat generated, a fraction is lost to surroundings through convection and radiation from the top and bottom (only-PV) of the panel and can be written as

$$q_{L,t} = h_t [T_{PV,t} - T_a] + \sigma \epsilon_t F_{ts} [T_{PV,t}^4 - T_s^4] + \sigma \epsilon_t F_{tg} [T_{PV,t}^4 - T_g^4] \tag{2}$$

$$q_{L,b} = h_b [T_{PV,b} - T_a] + \sigma \epsilon_b F_{bs} [T_{PV,b}^4 - T_s^4] + \sigma \epsilon_b F_{bg} [T_{PV,b}^4 - T_g^4] \text{ for Only-PV system} \tag{3}$$

where  $h_t$  and  $h_b$  are the convective heat transfer coefficients (natural ( $h_{t,n}$  and  $h_{b,n}$ ) and forced ( $h_{t,f}$  and  $h_{b,f}$ ) combined) of the top and bottom surfaces of the PV respectively and  $T_{PV,t}$  and  $T_{PV,b}$  are the corresponding temperatures.  $T_a$  is the ambient temperature,  $\sigma$  is the Stefan-Boltzmann constant,  $\epsilon_t$  (0.85 [41]) and  $\epsilon_b$  (0.91 [41]) are the emissivities of the top and bottom surfaces of the PV for long wavelength radiation,  $F_{ts}$ ,  $F_{tg}$ ,  $F_{bs}$  and  $F_{bg}$  are the view factors of the top and bottom surfaces of the PV to sky and ground respectively.  $T_s$  and  $T_g$  are the sky and ground temperatures respectively. The first term of the above equations (Eqs. (2) and (3)) represents the heat loss from the PV due to convection. The second and third terms are the radiative heat losses from PV to sky and ground respectively based on the corresponding view factors.  $h_{t,n}$  and  $h_{b,n}$  can be determined by  $Nu k_a / L_{ch}$ .  $k_a$  is the thermal conductivity of air and  $L_{ch}$  (characteristic length) is the surface length along the air flow direction. Nusselt numbers for top ( $Nu_t$ ) and back ( $Nu_b$ ) can be written as follows [42].

$$Nu_t = \begin{cases} [0.13(Ra)^{1/3} - (Gr_c Pr)^{1/3}] + 0.56(Gr_c Pr \sin \beta)^{1/4}; & \text{if } \beta > 30^\circ \\ [0.13(Ra)^{1/3}]; & \text{if } \beta \leq 30^\circ \end{cases} \tag{4}$$

$$Nu_b = \begin{cases} 0.58(Ra)^{1/5}; & \text{if } \beta \leq 2^\circ \\ 0.56(Ra \sin \beta)^{1/5}; & \text{if } 2^\circ < \beta < 30^\circ \\ \left[ 0.825 + \frac{0.387(Ra \sin \beta)^{1/6}}{\{1 + (0.492 / Pr)^{9/16}\}^{2/7}} \right]^2; & \text{if } \beta \geq 30^\circ \end{cases} \tag{5}$$

where  $Pr$  is the Prandtl number of air,  $Gr_c$  is the critical Grashof number =  $1.327 \times 10^{10} \exp\{-3.708 (\pi/2 - \beta)\}$  and  $Ra$  is the Rayleigh number which is given by

$$Ra = \frac{g(T_{t,avg} - T_a)L_{ch}^3 Pr}{(0.25T_{t,avg} + 0.75T_a)v^2} \tag{6}$$

In the above expressions, all the physical properties are defined at a temperature equals to  $0.75T_{t,avg} + 0.25T_a$  [41]. The correlations of  $h_{t,f}$  and  $h_{b,f}$  with wind velocity ( $v_w$ ) can be given by

$$h_{t,f} = 0.848 k [\sin \beta \cos \gamma_w v_w Pr / v]^{0.5} (L_{ch}/2)^{-0.5} \tag{7}$$

$$h_{b,f} = \begin{cases} 5.74 v_w^{0.8} L_{ch}^{-0.2}; & \text{if } x_c/L_{ch} \leq 0.05 \\ 5.74 v_w^{0.8} L_{ch}^{-0.2} - 16.46 L_{ch}^{-1}; & \text{if } 0.05 < x_c/L_{ch} < 0.95 \\ 3.83 v_w^{0.5} L_{ch}^{-0.5}; & \text{if } x_c/L_{ch} \geq 0.95 \end{cases} \tag{8}$$

where  $\gamma_w$  is the angle defining the wind direction [42] and  $x_c$  is the

critical length. In Eq. (8), the first correlation corresponds to the fully turbulent flow when critical length is very small compared to the characteristic length, third correlation is for laminar flow when the ratio of critical to characteristic length is greater than or equal to 0.95 and the second correlation corresponds to mixed flow considering the transition from laminar to turbulent.  $x_c$  can be calculated using the following relation

$$x_c = \frac{Re_c v}{v_w} \tag{9}$$

where  $Re_c$  is the critical Reynolds number (=  $4 \times 10^5$ ).

The governing equations for the system can be described as follows.

### 2.1. PV and aluminium container with fins

In order to calculate the temperature of any  $j^{th}$  layer of the PV and the aluminium container with fins in  $x$  and  $y$  directions at any time  $t$ , the following equation can be solved

$$\rho c_p \frac{\partial T}{\partial t} = k \left( \frac{\partial^2 T}{\partial x^2} + \frac{\partial^2 T}{\partial y^2} \right) + G_{PV} \tag{10}$$

with boundary conditions

$$k_{gl} \frac{\partial T_{gl}}{\partial y} = q_{L,t} \text{ at top surface of glass} \tag{11}$$

$$k_{ted} \frac{\partial T_{ted}}{\partial y} = \begin{cases} q_{L,b} \text{ at bottom surface of tedlar for Only-PV system} \\ k_{al} \frac{\partial T_{al}}{\partial y} \text{ at interface of tedlar and aluminium} \end{cases} \tag{12}$$

$$k_{PV,j} \frac{\partial T_{PV,j}}{\partial y} = k_{PV,j+1} \frac{\partial T_{PV,j+1}}{\partial y} \text{ at interface of } j^{th} \text{ and } (j+1)^{th} \text{ layer of PV} \tag{13}$$

$$k_{al} \frac{\partial T_{al}}{\partial y} = k_p \frac{\partial T_p}{\partial y} \text{ at interfaces of aluminium and PCM normal to } y \text{ axis} \tag{14}$$

$$k_{al} \frac{\partial T_{al}}{\partial x} = k_p \frac{\partial T_p}{\partial x} \text{ at interfaces of aluminium and PCM normal to } x \text{ axis} \tag{15}$$

$$k \frac{\partial T}{\partial x} = 0 \text{ at both side walls of system} \tag{16}$$

$$k_{al} \frac{\partial T_{al}}{\partial y} = 0 \text{ at bottom of system} \tag{17}$$

$$T = T_a \text{ at } t = 0 \tag{18}$$

where  $\rho$ ,  $c_p$ ,  $T$ ,  $k$  and  $G_{PV}$  are the density, specific heat capacity, temperature, thermal conductivity and heat generation in PV respectively. Eq. (11) conveys that the rate of heat leaving the top surface of the glass layer is same as the rate of heat loss from the top of the system. Eq. (12) explains that the rate of heat leaving the bottom surface of the tedlar is same as the rate of heat loss from the bottom of the only-PV system and is equal to the rate of heat entering the top surface of the aluminium container for other systems. Eq. (13) explains that the rate of heat leaving the  $j^{th}$  PV layer from its bottom surface is equal to the rate of heat entering the  $(j+1)^{th}$  layer from its top surface. Eqs. (14) and (15) explain that at the interfaces of aluminium and PCM, the rate of heat leaving the aluminium is equal to the rate of heat entering the PCM. Eqs. (16) and (17) explain that the rate of heat leaving the side walls of the system and the bottom of the aluminium container is nil as they are insulated. Eq. (18) explains that, initially, the temperature of the system is same as that of the ambient.

## 2.2. PCM

RT 25 HC PCM [43] has been chosen for the current work. In order to calculate the phase change material's temperature and the velocities in  $x$  and  $y$  directions at any time  $t$ , following equations can be solved

$$\rho_P c_{p,P} \frac{\partial T_P}{\partial t} = \frac{\partial}{\partial x} \left( k_P \frac{\partial T_P}{\partial x} - \rho_P c_{p,P} u_x T_P \right) + \frac{\partial}{\partial y} \left( k_P \frac{\partial T_P}{\partial y} - \rho_P c_{p,P} u_y T_P \right) \quad (19)$$

$$\rho_P \left( \frac{\partial u_x}{\partial t} + u_x \frac{\partial u_x}{\partial x} + u_y \frac{\partial u_x}{\partial y} \right) = -\frac{\partial p}{\partial x} + \mu \left( \frac{\partial^2 u_x}{\partial x^2} + \frac{\partial^2 u_x}{\partial y^2} \right) + \rho g_x \quad (20)$$

$$\rho_P \left( \frac{\partial u_y}{\partial t} + u_x \frac{\partial u_y}{\partial x} + u_y \frac{\partial u_y}{\partial y} \right) = -\frac{\partial p}{\partial y} + \mu \left( \frac{\partial^2 u_y}{\partial x^2} + \frac{\partial^2 u_y}{\partial y^2} \right) + \rho g_y \quad (21)$$

$$\frac{\partial u_x}{\partial x} + \frac{\partial u_y}{\partial y} = 0 \quad (22)$$

with boundary conditions

$$u_x = u_y = 0 \text{ at all walls inside PCM container} \quad (23)$$

$$u_x = u_y = 0 \text{ at } t = 0 \quad (24)$$

$$B_{\text{at } T = T_m - \frac{\Delta T}{2}} = \frac{dB}{dT} \Big|_{T_m - \frac{\Delta T}{2}} = \frac{d^2 B}{dT^2} \Big|_{T_m - \frac{\Delta T}{2}} = \frac{dB}{dT} \Big|_{T_m + \frac{\Delta T}{2}} = \frac{d^2 B}{dT^2} \Big|_{T_m + \frac{\Delta T}{2}} = 0, B_{T_m + \frac{\Delta T}{2}} = 1, B_{T_m} = \frac{1}{2} \quad (33)$$

$$T_P = T_a \text{ at } t = 0 \quad (25)$$

where  $u_x$  and  $u_y$  are the phase change material velocities in  $x$  and  $y$  directions respectively,  $p$  is pressure,  $\mu$  is dynamic viscosity and  $g_x$  and  $g_y$  are gravitational accelerations in  $x$  and  $y$  directions respectively. PCM follows the no-slip condition (Eq. (23)) which conveys that the PCM velocities in  $x$  and  $y$  directions at all walls inside the PCM container are 0 m/s. Eqs. (24) and (25) convey that, initially, the PCM velocity is nil and the temperature is same as that of the ambient.  $\rho g_x$  and  $\rho g_y$  (Eqs. (20) and (21)) represent the buoyancy forces which can be expressed as follows

$$\rho g_x = \rho_{P,l} [1 - \beta_c (T_P - T_m)] g_x \quad (26)$$

$$\rho g_y = \rho_{P,l} [1 - \beta_c (T_P - T_m)] g_y \quad (27)$$

where  $\rho_{P,l}$ ,  $\beta_c$  and  $T_m$  are the density of the phase change material in liquid phase, expansion coefficient of the PCM due to temperature and the PCM melting temperature respectively.

The abrupt changes in the phase change material's thermal properties while undergoing phase change have to be dealt with carefully to get the convergence of the results. The same can be done using Biwole et al. [30] with proposed two functions for smooth accounting of the sharp fluctuations as

$$c_{p,P}(T) = c_{p,P,s} + (c_{p,P,l} - c_{p,P,s})B(T) + L_h D(T) \quad (28)$$

$$\rho_P(T) = \rho_{P,s} + (\rho_{P,l} - \rho_{P,s})B(T) \quad (29)$$

$$k_P(T) = k_{P,s} + (k_{P,l} - k_{P,s})B(T) \quad (30)$$

where  $B$  is the phase change material's liquid fraction and  $D$  is a function [30] used to distribute the latent heat ( $L_h$ ) of the PCM in the phase change zone. For the regions having PCM temperature lower than the solidification temperature ( $T_m - \Delta T/2$ ), the PCM is in solid phase resulting in liquid fraction ( $B$ ) and  $D$  as 0 leading to  $c_{p,P} = c_{p,P,s}$ ,  $\rho_P = \rho_{P,s}$  and  $k_P = k_{P,s}$ . The portions where PCM temperature is above liquidification temperature ( $T_m + \Delta T/2$ ), the PCM is in liquid phase resulting in liquid fraction ( $B$ ) and  $D$  as 1 and 0 respectively leading to  $c_{p,P} = c_{p,P,l}$ ,  $\rho_P = \rho_{P,l}$  and  $k_P = k_{P,l}$ . The abrupt changes in the viscosity of the PCM ( $\mu$ )

can be modelled as [31].

$$\mu(T) = \mu_l \left[ 1 + \frac{C \{1 - B(T)\}^2}{B(T)^3 + q} \right] \quad (31)$$

As explained by Biwole et al. [30],  $C$  changes its value depending upon the morphology of the medium. Higher values of  $C$  result in the reduction of flow of liquid matter in the mushy zone. A value of  $10^5$  [30] is experimentally verified for RT 25 HC. A very low value of  $q$  ( $10^{-3}$ ) has been used by Biwole et al. [30] in order to keep the above correlation valid even for solid regions of PCM. The same values have been chosen for the current study. For the regions having PCM temperature lower than the solidification temperature ( $T_m - \Delta T/2$ ), the above correlation provides a very high value of viscosity for PCM which helps it to behave like a solid. The portions where PCM temperature is above liquidification temperature ( $T_m + \Delta T/2$ ), the PCM is in liquid phase resulting in liquid fraction ( $B$ ) as 1 leading to  $\mu = \mu_l$ .

To ease the convergence, the liquid fraction ( $B$ ) during phase change is modelled as a second order continuous differentiable function as follows

$$B(T) = \sum_{i=0}^6 a_i T^i \quad (32)$$

These conditions (Eq. (33)) give the coefficients ( $a_i$ ) of Eq. (32) as follows:

$$\begin{bmatrix} a_0 \\ a_1 \\ a_2 \\ a_3 \\ a_4 \\ a_5 \\ a_6 \end{bmatrix} = \begin{bmatrix} 1 & b & b^2 & b^3 & b^4 & b^5 & b^6 \\ 0 & 1 & 2b & 3b^2 & 4b^3 & 5b^4 & 6b^5 \\ 0 & 0 & 2 & 6b & 12b^2 & 20b^3 & 30b^4 \\ 0 & 1 & 2c & 3c^2 & 4c^3 & 5c^4 & 6c^5 \\ 0 & 0 & 2 & 6c & 12c^2 & 20c^3 & 30c^4 \\ 1 & c & c^2 & c^3 & c^4 & c^5 & c^6 \\ 1 & d & d^2 & d^3 & d^4 & d^5 & d^6 \end{bmatrix}^{-1} \begin{bmatrix} 0 \\ 0 \\ 0 \\ 0 \\ 0 \\ 1 \\ 0.5 \end{bmatrix} \quad (34)$$

where  $b = T_m - \Delta T/2$ ,  $c = T_m + \Delta T/2$  and  $d = T_m$   
 $D$  in Eq. (28) can be given by

$$D(T) = \frac{e^{-(T-T_m)^2/(\Delta T/4)^2}}{\sqrt{\pi(\Delta T/4)^2}} \quad (35)$$

## 3. Solution procedure

ANSYS Fluent 17.1 has been used to solve the equations. Mesh has been generated using quadrilateral grid. The grid independence study shows that any further reduction in the distance between the successive nodes beyond 1 mm does not lead to significant improvement in the results. The accepted residuals of the energy, continuity and velocity have been chosen as  $10^{-8}$ ,  $10^{-4}$  and  $10^{-4}$  respectively because the decrease in the accepted value of the energy residual from  $10^{-6}$  to  $10^{-7}$ ,  $10^{-7}$  to  $10^{-8}$  and  $10^{-8}$  to  $10^{-9}$  changes the temperature of system maximally by 3.1%, 0.5% and 0.0% respectively.

## 4. Experimental verification

In order to verify the presented model with the experimental measurements, the values reported by Huang et al. [44] have been taken. RT 25 HC phase change material was considered. The  $I_T$  and  $T_a$  were  $750 \text{ W/m}^2$  and  $20^\circ \text{C}$  respectively. The top and bottom of the system were not insulated whereas the side walls were insulated. Using the proposed model, the similar system has been simulated. The variation

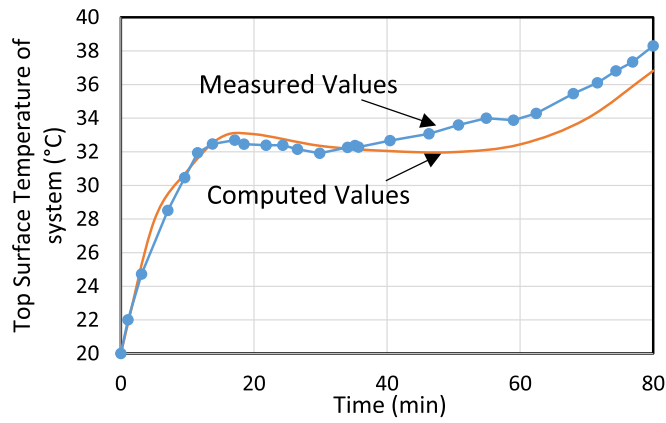


Fig. 2. Verification of the model against the experimental measurements [29].

**Table 1**  
Properties of different layers of PV and aluminium.

Material	Thermal Conductivity (W/mK)	Heat Capacity (kJ/kgK)	Density (kg/m <sup>3</sup> )	Thickness (mm)
Glass	1.8	0.5	3000	3
EVA	0.35	2.1	960	0.5
Silicon	148	0.68	2330	0.3
Tedlar	0.2	1.25	1200	0.1
Aluminium	211	0.9	2675	4

in the surface temperature of the top of the system with time is shown in Fig. 2 and compared with the experimental measurements. The mismatch lies between -2.0 °C and +0.7 °C.

### 5. Results and discussion

Based on the proposed methodology, the thermal response of the Finned-PV-PCM system in terms of temperature variations with time have been studied and analysed for range of spacing between fins, fin

**Table 2**  
Properties of RT 25 HC phase change material and other variables.

Parameter	Value
$c_{p,p,s}$ (kJ/kgK)	1.8
$c_{p,p,l}$ (kJ/kgK)	2.4
$I_T$ (W/m <sup>2</sup> )	750
$k_{p,s}$ (W/mK)	0.19
$k_{p,l}$ (W/mK)	0.18
$L$ (m)	1
$L_f$ (cm)	3
$L_h$ (kJ/kg)	232
$s_f$ (cm)	33
$T_a$ (°C)	20
$t_f$ (mm)	4
$T_m$ (°C)	26.6
$v_w$ (m/s)	4
$\beta$ (°)	45
$\beta_c$ (K <sup>-1</sup> )	0.001
$\gamma_w$ (°)	0
$\delta$ (cm)	3
$\Delta T$ (°C)	2
$\epsilon_r$	0.85
$\epsilon_b$	0.91
$\mu_s$ (kg/m-s)	$1.8 \times 10^5$
$\mu_l$ (kg/m-s)	0.001798
$\rho_{p,s}$ (kg/m <sup>3</sup> )	785
$\rho_{p,l}$ (kg/m <sup>3</sup> )	749
$(\tau\alpha)_{eff}$	0.9

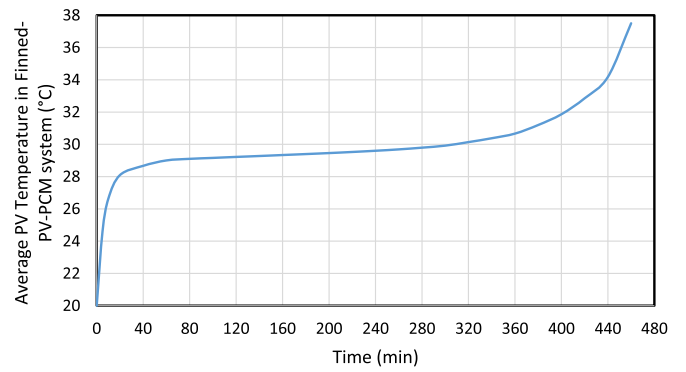


Fig. 3. PV temperature in Finned-PV-PCM system and its variation with time.

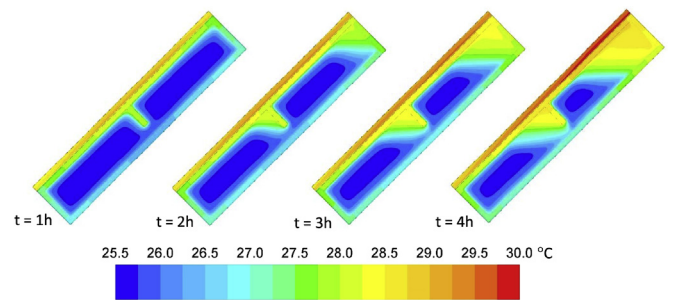


Fig. 4. Temperature of Finned-PV-PCM system and the melting process of PCM.

length, fin thickness and depth of the PCM box. The most suitable dimensions of fins and depths of container for various daily solar radiation values to optimally cool the PV have been calculated. The impact of fin dimensions on the suitable depth has also been investigated. Parameters used and the corresponding values for the calculations are tabulated in Tables 1 and 2.

The variation in average PV temperature with time in Finned-PV-PCM system is presented in Fig. 3 and the variation in the temperature of the whole system is presented in Fig. 4. The results suggest that there is an initial surge in PV temperature which eventually saturates and then remains constant for significant time. It witnesses an increase again beyond a point. It is due to the fact that firstly, the rate of heat extraction by PCM is low due to its solid phase. As soon as the phase change material starts to melt, it starts absorbing heat (latent) from photovoltaic without any rise in temperature. Once the phase change material is fully melted and has absorbed all the latent heat, there is

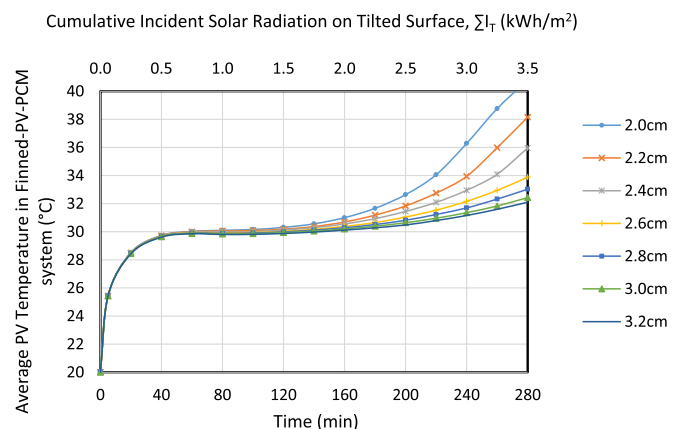


Fig. 5. PV temperature in Finned-PV-PCM for different depths of box containing phase change material.

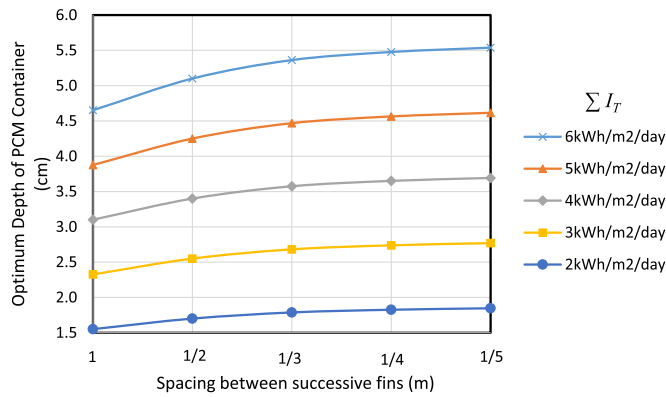


Fig. 6. Optimum depths of phase change material container for different spacings between fins and solar radiation levels.

observed a decrease in the rate of heat extraction because heat that is now being extracted is only sensible leading to further rise in PV temperature.

5.1. Optimum depth of phase change material container

The variations in average PV temperature (in Finned-PV-PCM system) are shown in Fig. 5 for different depths of box containing phase change material. It is observed that with increase in depth of PCM box, the cooling capacity in terms of duration increases. However, beyond a limit, it does not lead to significant capacity addition. For example, for  $\Sigma I_T = 3 \text{ kWh/m}^2/\text{day}$ , if the depth is increased beyond 2.8 cm, PV can't be cooled more than 1 °C. Thus, 2.8 cm can be considered as the most suitable depth for  $\Sigma I_T = 3 \text{ kWh/m}^2/\text{day}$ .

5.1.1. Effect of spacing between fins on optimum depth of phase change material container

The most suitable depths are calculated for various spacings between successive fins and various daily solar irradiance and the values are shown in Fig. 6. The results show that for a system having spacing as 100 cm, the suitable depth of container is 3.9 cm for  $\Sigma I_T = 5 \text{ kWh/m}^2/\text{day}$ . It means that the PV temperature starts increasing again for  $\Sigma I_T$  greater than 5 kWh/m²/day. If spacing decreases to 25 cm, the suitable depth increases to 4.6 cm. It is due to the fact that, for smaller spacing, number of fins in the system are larger and heat extraction rate of phase change material is higher and, thus, it melts in shorter duration. Thus, for smaller spacing between fins, larger quantity of phase change material is required to maintain PV at lower temperature.

It must be noted that, in the current work, very less number of fins are introduced in the container. Thus, the PCM mass diminished by fins is negligible.

It must also be noted that if spacing between fins is increased beyond a point, the convective energy flow inside the PCM container reduces and conductive energy flow increases which may lead to decrease in the rate of melting with decrease in spacing.

5.1.2. Effect of length of fins on optimum depth of phase change material container

The thermal variations of Finned-PV-PCM system are analysed for different depths of phase change material box. The most suitable depths are calculated for various lengths of fins and various daily solar irradiance and the values are shown in Fig. 7. It is observed that for a system having  $L_f$  as  $\delta/3$ , the suitable depth of container is 4.0 cm for  $\Sigma I_T = 5 \text{ kWh/m}^2/\text{day}$ . It conveys that the PV temperature starts increasing again for  $\Sigma I_T$  greater than 5 kWh/m²/day. If  $L_f$  increases to  $\delta$ , the suitable depth increases to 4.5 cm. It is again due to faster rate of heat extraction leading to melting of PCM in shorter duration. Thus, for larger fin length, larger quantity of phase change material is required to

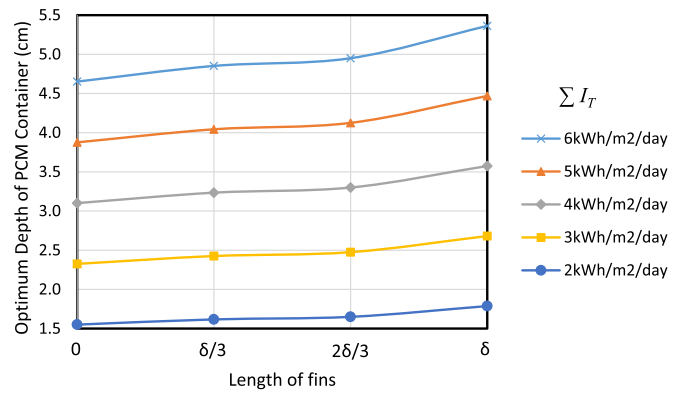


Fig. 7. Optimum depths of phase change material container for different lengths of fins and solar radiation levels.

cool the photovoltaic for desired time. It must also be noted that for a system having large number of fins, the increase in fin length can restrict the flow of melted PCM which may reduce the energy flow due to convection inside the phase change material container. Thus, it may happen that the increase in the fin length adversely affects the melting rate of the phase change material.

5.1.3. Effect of thickness of fins on optimum depth of phase change material container

The temperature patterns of Finned-PV-PCM system are analysed for different depths of container. The most suitable depths are calculated for various thicknesses of fins and various daily solar irradiance and the values are shown in Fig. 8. It is observed that for a system having  $t_f = 0.5 \text{ mm}$ , the suitable depth of container is 4.1 cm for  $\Sigma I_T = 5 \text{ kWh/m}^2/\text{day}$ . It conveys that the PV temperature starts increasing again for  $\Sigma I_T$  greater than 5 kWh/m²/day. If  $t_f$  increases to 2 mm, the suitable depth increases to 4.5 cm. Thus, the results show that for thicker fins, the suitable depths of PCM box are larger which is caused by early melting of PCM due to higher heat extraction rate thereby requiring more phase change material depth for effective cooling of PV.

5.2. Effect of fins on the standard deviation of PV temperature along height

The results (Fig. 4) show that when some portion of the PCM melts, the solid portion is displaced downwards pushing the liquid portion upwards. It leads to thermal variation inside the PCM container along the height resulting in temperature variations in the PV. The standard deviation of the PV temperature (along the height) is calculated for various spacings between fins and presented in Fig. 9. The results show that as spacing between fins decreases, the standard deviation of the PV

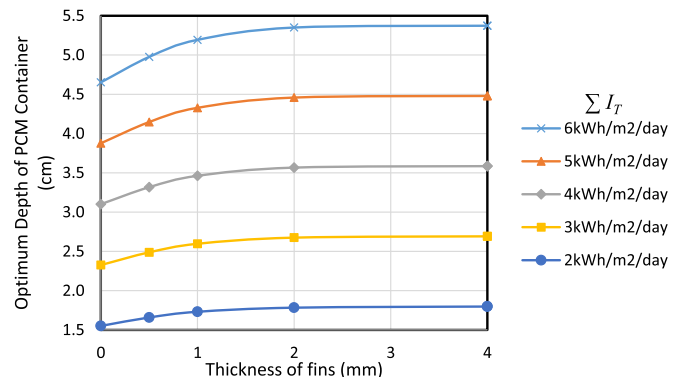


Fig. 8. Optimum depths of phase change material container for different thicknesses of fins and solar radiation levels.

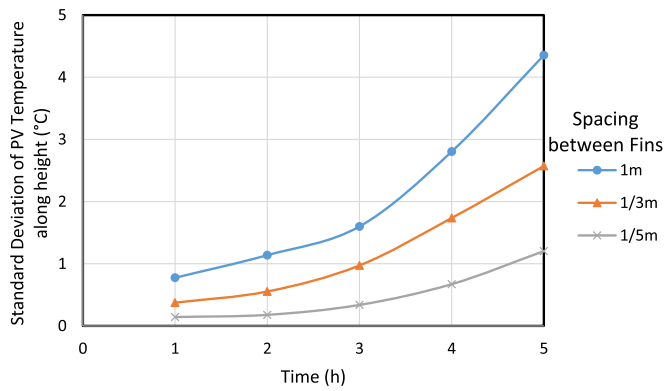


Fig. 9. Variation in standard deviation of the PV temperature (along the height) with time.

temperature decreases. It is due to the fact that, for a system having lesser spacing between fins, the displacement of solid portion of PCM (during melting process) is more restricted which leads to lesser temperature variations inside the PCM container along the height resulting in lesser standard deviation of PV temperature.

The results also show that the standard deviation increases with time. It is due to the fact that, initially, the whole PCM is in solid phase leading to lesser thermal variations along the height and, thus, lesser standard deviation. As phase change material starts melting, the solid portion of PCM starts getting displaced downwards leading to increase in temperature variation along the height inside the PCM container.

It must also be noted that, when PCM becomes fully liquid, the temperature variation along the height will decrease.

### 5.3. Optimum spacing between fins

The variations in the average temperature of photovoltaic (in Fined-PV-PCM system) are shown in Fig. 10 for various spacings between successive fins and the corresponding heat extraction rate of phase change material has been presented in Fig. 11. The results show that as spacing decreases, temperature of PV decreases. It is due to the fact that with decrease in spacing, number of fins in the system increases which enhances the rate of heat extraction from PV (Fig. 11) leading to decrease in PV temperature. The results also show that decrease in spacing beyond 25 cm (1/4 m) does not lead to significant decrease in PV temperature. Thus, the best spacing between fins is 25 cm.

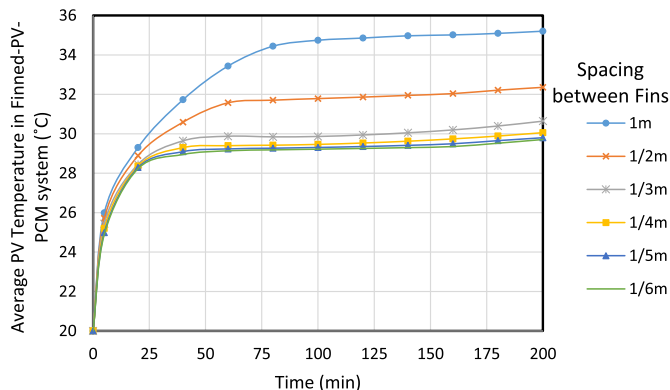


Fig. 10. PV temperature in Fined-PV-PCM system for various spacings between successive fins.

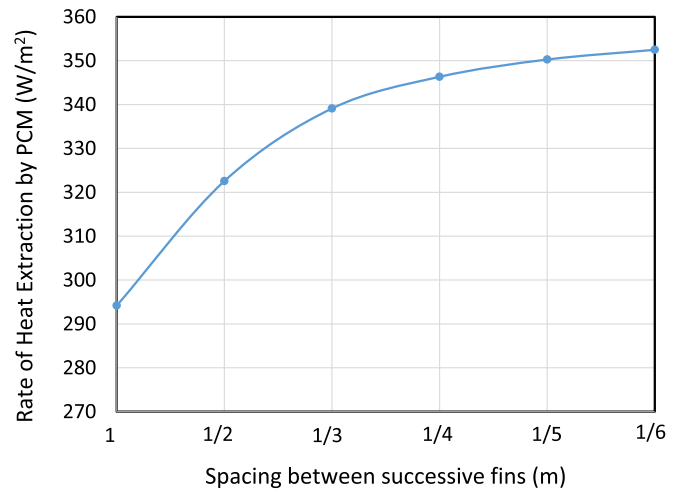


Fig. 11. Heat extraction rate of phase change material for various spacings between fins at t = 150 min.

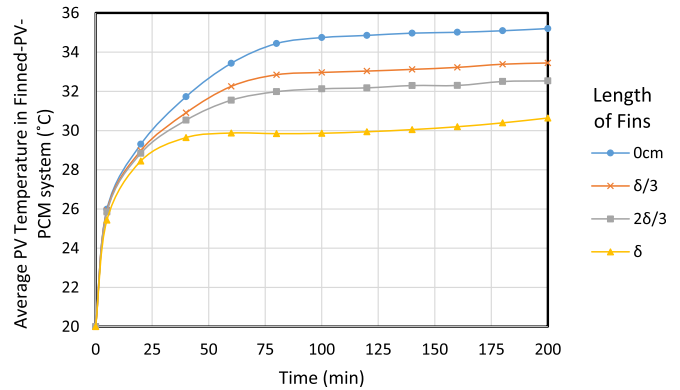


Fig. 12. PV temperature in Fined-PV-PCM system for different lengths of fins.

### 5.4. Optimum length of fins

The variations in the average temperature of photovoltaic (in Fined-PV-PCM system) are shown in Fig. 12 for different lengths of fins. The results show that the photovoltaic temperature decreases with increase in fin length. It happens due to faster rate of heat extraction from PV in case of longer fins (Fig. 13). The results also show that there

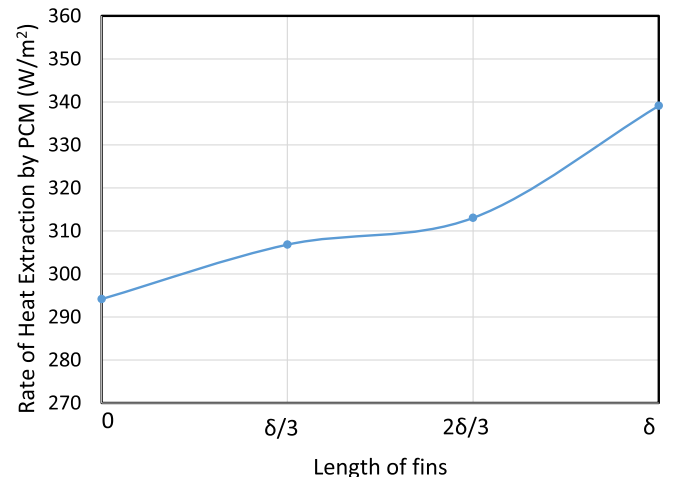


Fig. 13. Heat extraction rate of phase change material for various lengths of fins at t = 150 min.

is a significant decrement in PV temperature when fin length becomes  $\delta$  (depth of container) as compared to smaller lengths of fins. The reason for this sharp characteristic can be explained as follows. In case of fin length becoming  $\delta$ , the tip of the fin touches the bottom of container. Due to high conductivity of aluminium, the temperature at the bottom increases and then the PCM starts extracting heat from bottom also in addition to top and fins. Thus it leads to higher heat extraction rate of phase change material resulting in more cooling. Thus, the best length of fin is equal to the depth of container.

### 5.5. Optimum thickness of fins

The variations in the average temperature of photovoltaic (in Finned-PV-PCM system) are shown in Fig. 14 for different thicknesses of fins and the corresponding heat extraction rate of phase change material has been presented in Fig. 15. The results suggest the decrease in PV temperature with increase in fin thickness. It is again because of the previous reason of faster rate of heat extraction which happens in thicker fins (Fig. 15). The results also show that increase in thickness beyond 2 mm does not lead to significant decrease in photovoltaic temperature. Thus, the best thickness of fins is 2 mm.

## 6. Conclusions

A mathematical model is presented for analysing the thermal

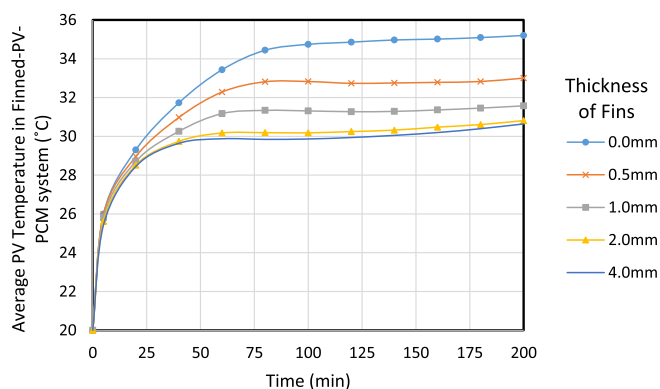


Fig. 14. PV temperature in Finned-PV-PCM system for different thicknesses of fins.

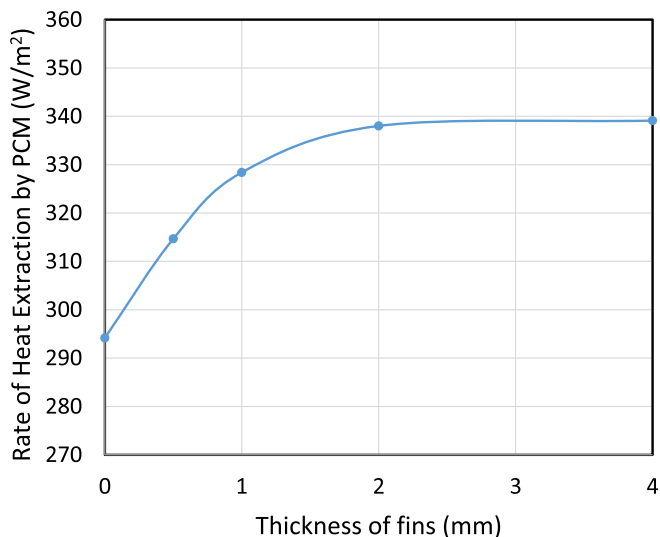


Fig. 15. Heat extraction rate of phase change material for various thicknesses of fins at  $t = 150$  min.

performance of PV, PV-PCM and Finned-PV-PCM systems accounting heat transfer via conduction, convection and radiation. To ensure the convergence, a 2nd order continuous and differentiable function is defined during the phase transition of the PCM. The model has been validated against the experimental measurements. The mismatch lies between  $-2.0$  °C and  $+0.7$  °C. The temperature variations of the systems with time have been analysed along with the effects of spacing between fins, length and thickness of fins. The most suitable fin dimensions are calculated to maintain the PV at low temperature. It is also observed that by increasing the quantity of phase change material (i.e. the depth of PCM container), the duration can be increased for which photovoltaic can be cooled. The most suitable depths of PCM box are calculated for various fin dimensions and daily solar radiation levels. The conclusions are as follows.

- (i) For smaller spacing between fins, larger quantity of phase change material is required to maintain the photovoltaic at low temperature because PCM melts in shorter duration due to higher rate of heat extraction. Smaller spacing between fins can keep PV cooler. However, decrease in spacing beyond 25 cm does not lead to significant improvement.
- (ii) For larger fin length, larger quantity of phase change material is required to keep photovoltaic cooler. Larger length of fins can maintain the photovoltaic at lower temperature. Best fin length is the one when it touches the bottom of the container.
- (iii) For larger fin thickness, larger quantity of phase change material is required for effective cooling of PV. Larger thickness of fins would lead to lower PV temperature. However, increase in thickness beyond 2 mm does not lead to much improvement.

It must be noted that, (i) in the current work, the optimum quantities of PCM are reported for cumulative incident solar radiation over the day. However, it may happen that the two locations with similar ambient conditions and cumulative incident solar radiation have different radiation distributions over the day which would lead to slightly different values of optimum PCM quantity in reality, (ii) the contact between the PV back and the aluminium container is considered to be perfect. However, in reality, the imperfect contact would reduce the heat transfer and (iii) the current work does not incorporate the effect of crystalline segregation of the PCM which can reduce the heat transfer within the PCM.

### Acknowledgment

The authors gratefully acknowledge the financial support from EPSRC-DST funded Reliable and Efficient System for Community Energy Solution - RESCUES project (EP/K03619X/1). In support of open access research, all underlying article materials (such as data, samples or models) can be accessed upon request via email to the corresponding author.

### Appendix A. Supplementary data

Supplementary data related to this article can be found at <http://dx.doi.org/10.1016/j.ijthermalsci.2018.04.033>.

### References

- [1] E. Skoplaki, J.A. Palyvos, On the temperature dependence of photovoltaic module electrical performance: a review of efficiency/power correlations, *Sol Energy* 83 (2009) 614–624.
- [2] M.J. Huang, P.C. Eames, B. Norton, Phase change materials for limiting temperature rise in building integrated photovoltaics, *Sol Energy* 80 (2006) 1121–1130.
- [3] A. Hasan, S.J. McCormack, M.J. Huang, B. Norton, Evaluation of phase change materials for thermal regulation enhancement of building integrated photovoltaics, *Sol Energy* 84 (2010) 1601–1612.
- [4] Y.S. Indartono, A. Suwono, F.Y. Pratama, Improving photovoltaics performance by using yellow petroleum jelly as phase change material, *Int J Low Carbon Technol* 0

- (2014) 1–5.
- [5] H. Mahamudul, M.M. Rahman, H.S.C. Metselaar, S. Mekhilef, S.A. Shezan, R. Sohel, et al., Temperature regulation of photovoltaic module using phase change material: a numerical analysis and experimental investigation, *Int J Photoenergy* (2016) 1–8 5917028.
- [6] J. Park, T. Kim, S.B. Leigh, Application of a phase-change material to improve the electrical performance of vertical-building-added photovoltaics considering the annual weather conditions, *Sol Energy* 105 (2014) 561–674.
- [7] A. Hasan, S.J. McCormack, M.J. Huang, J. Sarwar, B. Norton, Increased photovoltaic performance through temperature regulation by phase change materials: materials comparison in different climates, *Sol Energy* 115 (2015) 264–276.
- [8] A. Hasan, J. Sarwar, H. Alnoman, S. Abdelbaqi, Yearly energy performance of a photovoltaic-phase change material (PV-PCM) system in hot climate, *Sol Energy* 146 (2017) 417–429.
- [9] S. Sharma, A. Tahir, K.S. Reddy, T.K. Mallick, Performance enhancement of a Building-Integrated Concentrating Photovoltaic system using phase change material, *Sol Energy Mater Sol Cells* 149 (2016) 29–39.
- [10] M.J. Huang, P.C. Eames, B. Norton, N.J. Hewitt, Natural convection in an internally finned phase change material heat sink for the thermal management of photovoltaics, *Sol Energy Mater Sol Cells* 95 (2011) 1598–1603.
- [11] M.C. Browne, K. Lawlor, A. Kelly, B. Norton, S.J. McCormack, Indoor characterisation of a photovoltaic/thermal phase change material system, *Energy Procedia* 70 (2015) 163–171.
- [12] M.C. Browne, D. Quigley, H.R. Hard, S. Gilligan, N.C.C. Ribeiro, N. Almeida, et al., Assessing the thermal performance of phase change material in a photovoltaic/thermal system, *Energy Procedia* 91 (2016) 113–121.
- [13] F. Hachem, B. Abdulhay, M. Ramadan, H. El Hage, M.G. El Rab, M. Khaled, Improving the performance of photovoltaic cells using pure and combined phase change materials - experiments and transient energy balance, *Renew Energy* 107 (2017) 567–575.
- [14] M.C. Browne, B. Norton, S.J. McCormack, Phase change materials for photovoltaic thermal management, *Renew Sustain Energy Rev* 47 (2015) 762–782.
- [15] T. Ma, H. Yang, Y. Zhang, L. Lu, X. Wang, Using phase change materials in photovoltaic systems for thermal regulation and electrical efficiency improvement: a review and outlook, *Renew Sustain Energy Rev* 43 (2015) 1273–1284.
- [16] D. Du, J. Darkwa, G. Kokogiannakis, Thermal management systems for Photovoltaics (PV) installations: a critical review, *Sol Energy* 97 (2013) 238–254.
- [17] A. Shukla, K. Kant, A. Sharma, P.H. Biwole, Cooling methodologies of photovoltaic module for enhancing electrical efficiency: a review, *Sol Energy Mater Sol Cells* 160 (2017) 275–286.
- [18] S.S. Chandel, T. Agarwal, Review of cooling techniques using phase change materials for enhancing efficiency of photovoltaic power systems, *Renew Sustain Energy Rev* 73 (2017) 1342–1351.
- [19] V.L. Brano, G. Ciulla, A. Piacentino, F. Cardona, Finite difference thermal model of a latent heat storage system coupled with a photovoltaic device: description and experimental validation, *Renew Energy* 68 (2014) 181–193.
- [20] P. Atkin, M.M. Farid, Improving the efficiency of photovoltaic cells using PCM infused graphite and aluminium fins, *Sol Energy* 114 (2015) 217–228.
- [21] C.J. Smith, P.M. Forster, R. Crook, Global analysis of photovoltaic energy output enhanced by phase change material cooling, *Appl Energy* 126 (2014) 21–28.
- [22] M.A. Kibria, R. Saidur, F.A. Al-Sulaiman, M.M.A. Aziz, Development of a thermal model for a hybrid photovoltaic module and phase change materials storage integrated in buildings, *Sol Energy* 124 (2016) 114–123.
- [23] K. Kant, A. Shukla, A. Sharma, P.H. Biwole, Heat transfer studies of photovoltaic panel coupled with phase change material, *Sol Energy* 140 (2016) 151–161.
- [24] M.J. Huang, P.C. Eames, B. Norton, Thermal regulation of building-integrated photovoltaics using phase change materials, *Int J Heat Mass Tran* 47 (2004) 2715–2733.
- [25] C.J. Ho, A.O. Tanuwijaya, C.M. Lai, Thermal and electrical performance of a BIPV integrated with a microencapsulated phase change material layer, *Energy Build* 50 (2012) 331–338.
- [26] M.J. Huang, The effect of using two PCMs on the thermal regulation performance of BIPV systems, *Sol Energy Mater Sol Cells* 95 (2011) 957–963.
- [27] S. Khanna, K.S. Reddy, T.K. Mallick, Performance analysis of tilted photovoltaic system integrated with phase change material under varying operating conditions, *Energy* 133 (2017) 887–899, <http://dx.doi.org/10.1016/j.energy.2017.05.150>.
- [28] S. Khanna, K.S. Reddy, T.K. Mallick, Climatic behaviour of solar photovoltaic integrated with phase change material, *Energy Convers Manag* 166 (2018) 590–601.
- [29] S. Khanna, K.S. Reddy, T.K. Mallick, Optimization of solar photovoltaic system integrated with phase change material, *Sol Energy* 163 (2018) 591–599.
- [30] P.H. Biwole, P. Eclache, F. Kuznik, Phase-change materials to improve solar panel's performance, *Energy Build* 62 (2013) 59–67.
- [31] D. Groulx, P.H. Biwole, Solar PV passive temperature control using phase change materials, 15<sup>th</sup> International Heat Transfer Conference, August 10–15, 2014, Kyoto, Japan (2014).
- [32] V. Shatikian, G. Ziskind, R. Letan, Numerical investigation of a PCM-based heat sink with internal fins, *Int J Heat Mass Tran* 48 (2005) 3689–3706.
- [33] V. Shatikian, G. Ziskind, R. Letan, Numerical investigation of a PCM-based heat sink with internal fins: constant heat flux, *Int J Heat Mass Tran* 51 (2008) 1488–1493.
- [34] S.K. Saha, P. Dutta, Role of melt convection on the thermal performance of heat sinks with phase change material, 10th Electronics packaging technology conference, 9–12 Dec. 2008 (2008).
- [35] K.C. Nayak, S.K. Saha, K. Srinivasan, P. Dutta, A numerical model for heat sinks with phase change materials and thermal conductivity enhancers, *Int J Heat Mass Tran* 49 (2006) 1833–1844.
- [36] R. Baby, C. Balaji, Experimental investigations on phase change material based finned heat sinks for electronic equipment cooling, *Int J Heat Mass Tran* 55 (2012) 1642–1649.
- [37] S.C. Fok, W. Shen, F.L. Tan, Cooling of portable hand-held electronic devices using phase change materials in finned heat sinks, *Int J Therm Sci* 49 (2010) 109–117.
- [38] L.W. Fan, Y.Q. Xiao, Y. Zeng, X. Fang, X. Wang, X. Xu, et al., Effects of melting temperature and the presence of internal fins on the performance of a phase change material (PCM)-based heat sink, *Int J Therm Sci* 70 (2013) 114–126.
- [39] Srikanth R., Balaji C., Experimental investigation on the heat transfer performance of a PCM based pin fin heat sink with discrete heating. *Int J Therm Sci* 111, 188–203.
- [40] P.H. Biwole, D. Groulx, F. Souayfane, T. Chiu, Influence of fin size and distribution on solid-liquid phase change in a rectangular enclosure, *Int J Therm Sci* 124 (2018) 433–446.
- [41] E. Kaplani, S. Kaplanis, Thermal modelling and experimental assessment of the dependence of PV module temperature on wind velocity and direction, module orientation and inclination, *Sol Energy* 107 (2014) 443–460.
- [42] S. Khanna, S. Sundaram, K.S. Reddy, T.K. Mallick, Performance analysis of perovskite and dye-sensitized solar cells under varying operating conditions and comparison with monocrystalline silicon cell, *Appl Therm Eng* 127 (2017) 559–565.
- [43] Rubitherm Phase Change Material. <https://www.rubitherm.eu/> (accessed 25.07.2017).
- [44] M.J. Huang, P.C. Eames, B. Norton, Comparison of predictions made using a new 3D phase change material thermal control model with experimental measurements and predictions made using a validated 2D model, *Heat Tran Eng* 28 (2007) 31–37.